BJES Basrah Journal for Engineering Sciences

Basrah Journal for Engineering Sciences, Vol. 23, No. 2, 2023, 11-19

Original Article

Journal homepage: www.bjes.edu.iq
ISSN (Online): 23118385, ISSN (Print): 18146120

Numerical Study the Effect of Cylinder Location on the Mixed Convection in an Open Square Cavity

Eman G. Mohammed[1,*] and Falah A. Abood[2]

[1, 2] *Department of Mechanical Engineering, College of Engineering, University of Basrah, Basrah, Iraq*
Email: eman.ghazi1995@gmail.com, falah.abood@uobasrah.edu.iq

Received: 16 September 2022; Accepted: 21 October 2022; Published: 30 December 2023

Abstract:– Mixed convection heat transfer of air in a horizontal channel with an open square cavity is studied numerically. At the center of the cavity, it is an insulated rotating circular cylinder for enhancing the efficiency of heat transmission, the location of the inner cylinder is changed vertically along the centerline of the cavity. Heat is applied to the bottom wall of the cavity at a constant temperature, and the other walls are adiabatic. The flow is steady-state, laminar, and incompressible. Using computational fluid dynamics (CFD) and the commercial software program FLUENT 2019 R1, the equations of continuity, momentum, and energy are numerically solved. The angular velocity of the cylinder range is ($0.5 \leq \omega \leq 4$) rad/sec in a counterclockwise direction, the Richardson number range ($Ri = 0.1, 1, 10$), Reynolds number is 100 and the cylinder location is ($C = 70, 50, 30$) mm. The airflow Prandtl number is taken as ($Pr = 0.7$). The effect of various positions of the rotating cylinder has been examined through the visualization of streamline and isotherm contour, as well as the distribution of the average Nusselt number of the heated surface. The results indicate that the flow field and temperature distributions inside the cavity are strongly dependent on the rotating circular cylinder and the position of the inner cylinder.

Keywords:– Mixed convection, Square cavity, Rotating cylinder, Vertical cylinder locations, Laminar flow.

http://doi.org/10.33971/bjes.23.2.2

1. Introduction

A fundamental fluid mechanics topic of great interest is the flow around a rotating circular cylinder, it could be applied to a variety of practical systems. Investigating enclosures with rotating or stationary obstacles has been carried out using a variety of numerical and experimental techniques [1–3].

Abood et al. (2011) [4] numerically analyzed the laminar heat transfer through mixed convection in a square hollow with an interior hot cylinder. The right vertical wall's temperature is maintained constant. For $Ri = 0 - 12$, $50 \leq Re \leq 200$, $Pr = 0.71$, and inlet position $hi = 0.2$, using the finite element method and a software package (FlexPDF) to solve governing equations. At the heated surface, for the highest value of Re and Ri, the average Nusselt number is the highest. The flow and heat fields are significantly affected by the position of the solid cylinder.

Alshara (2012) [5] analyzed numerically how rotating horizontal single or multiple cylinders influence mixed convection heat transfer in an air-filled, equilateral triangle. With the FlexPDE soft package, the finite element approach is numerically solved for incompressible, laminar, steady, two-dimensional flows. There are three cases: one rotating cylinder, three rotating cylinders moving in the same direction, and three rotating cylinders moving in three different directions. Prandtl number ($Pr = 0.7$), the Rayleigh number ($Ra = 10^2 - 10^5$), the dimensionless radius of the rotating cylinder ($R = 0.1 - 0.25$), and the dimensionless angular velocity ($\Omega = 0 - 1000$) (for both clockwise and counterclockwise directions). For the same ratio of the solid cylinder or cylinder volume to the entire enclosure volume, the average Nusselt number of a single rotating cylinder is higher than that of several rotating cylinders. It was observed that for all circumstances, raising Ra, R, and Ω results in an increase in the average Nusselt number for rotating cylinders, whether single or multiple.

Khanafer et al. (2013) [6] investigated the flow and heat transmission properties of mixed convection inside a lid-driven cavity containing a circular body. The effect of the Richardson number ($0.01 \leq Ri \leq 10$), non-dimensional cylinder radius, and cylinder position on transport processes is presented inside the cavity. A finite element formulation based on the Galerkin method of weighted residuals is applied. In comparison to a case without the cylinder, the results of this investigation show that including the cylinder increases the average Nusselt value. For various Richardson values, the best heat transmission results have been found when a cylinder is placed towards the bottom wall. For different Richardson values, the average Nusselt number rises as the radius of the cylinder increases.

Alshara et al. (2013) [7] studied mixed convection heat transfer of an enclosure with a rotating inner cylinder for laminar airflow. While the other walls and surfaces of the inner cylinder are adiabatic, the bottom wall is heated at a constant temperature. Using the FlexPDE program, the finite element approach is used to solve the conservation governing equations for continuity, momentum, and energy.

Richardson's number ($Ri = 0, 6, 10$), Reynolds number ($Re = 20, 50, 100$), Prandtl number ($Pr = 0.7$), the dimensionless angular velocity ($\Omega = 0 - 3$) and dimensionless radius of a rotating cylinder ($R = 0 - 0.3$). The study showed that the average Nusselt number improves with increasing Ri, Re, and R and decreases with increasing Ω.

Selimefendigil et al. (2014) [8] presented in the backward-facing phase geometry, a numerical investigation of a rotating cylinder and fluid flow properties under the influence of a magnetic dipole. The governing equations were solved using a commercial finite element code. The ranges of ($10 \leq Re \leq 200$), cylinder rotation angle ($-75 \leq \Omega \leq 75$), and the magnetic dipole strength ($0 \leq \gamma \leq 16$) are investigated. Magnetic dipole strength and cylinder rotation angles have been found to control the recirculation zones' length and size. At low Reynolds numbers, the Nusselt number range as a function of cylinder rotation was significant in this case.

Khanafer et al. (2019) [9] studied numerical simulations of mixed convection heat transfer inside a differentially heated cavity containing two rotating cylinders. Considering various parameters such as ($0.01 < Ri < 10$), ($Re = 100$ and 500), non-dimensional cylinder rotation ($0 < \omega < 100$), the cylinder radius to cavity height ratio r_o/H is assumed to be constant at 0.1, cylinder location, with a Prandtl number of 0.7. The governing equations were solved using a finite element formulation based just on the Galerkin method. Both the magnitude and direction of the cylinders' rotation speeds have a considerable impact on the flow pattern and isotherms. The position of the cylinders had no effect on the average Nusselt number.

Mehryan et al. (2019) [10] examined the effects of $Cu - Al_2O_3/water$ hybrid Nanofluid and $Al_2O_3/water$ Nanofluid on mixed convection induced by a heated oscillating cylinder inside a square cavity. The effects of a number of parameters, ($10^3 \leq Ra \leq 10^5$), ($Pr = 6.2$), nanoparticle volume fraction ($0 \leq \phi \leq 0.02$), the amplitude of the oscillation ($0.5R \leq A \leq 1.5R$) and the period of the cylinder's oscillation ($0.5 \leq f \leq 48$) were studied. Newtonian, incompressible, and viscous Nanofluids are assumed in all cases. The fluid flow is inside the laminar flow range. The Galerkin weighted residual finite element numerical approach is used to solve this study. As the Rayleigh number is small, the results show that moving the oscillating cylinder toward the top and bottom walls raises the average Nusselt number. The strength and size of the vortices increase as the Rayleigh number has increased from 10^4 to 10^6, due to a rise in the buoyancy force, which decreases the thickness of the thermal boundary layer around the surface of the cylinder. It is discovered that a simple $Al_2O_3/water$ Nanofluid has a higher natural convection heat transfer rate than a $Cu - Al_2O_3/water$ hybrid Nanofluid.

Salman et al. (2020) [11] studied experimentally turbulent mixed convection in an enclosure in the form of a semicircle with a rotating cylinder. The angular velocities (62.8, 83.73, 125.6) rad/s are positioned horizontally and vertically in the cavity, with Rayleigh numbers ($2.9 \times 10^8, 5 \times 10^8$). The heat transfers and fluid flow fields have increased as rotational speeds have increased, with high angular velocity and Reynolds numbers, promoting a local Nusselt number.

Selimefendigila et al. (2020) [12] studied numerically the mixed convection that occurs in a phase-changing material-filled square cavity, under the influence of a rotating cylinder. The horizontal walls are adiabatic, while vertical walls are controlled at fixed temperature. The effects of the cylinder's angular rotational speed ($-7.5, 7.5$), vertical location ($0.25, 0.75$), and two main cylinder sizes ($0.05, 0.1$). The finite element approach was used to solve the governing equations. It has been discovered that heat transport in the cavity could be controlled using rotating cylinder parameters. The angular rotational speed of the cylinder determines the maximum value of average heat transmission for various vertical locations of the cylinder. Average heat transmission increases by around 22.5 percent when the angular rotational speed of the cylinder is ($\omega = 7.5$) compared to a motionless cylinder ($\omega = 0$). Despite the extensive literature on open cavity research, there is still more work to be done in this field. Such as the study of the heat transmission process with mixed convection inside an enclosure with channels for fluid entry and exit. Created a study looking at the effect of rotation and vertical locations on the mixed convection heat transfer process in a channel with an open cavity, with the influence of parameter, Ri.

2. Theoretical analysis

2.1. Geometry description

The geometry of the channel including the square open cavity contains a rotating cylinder and the computational domain used in this study is shown in Fig. 1.

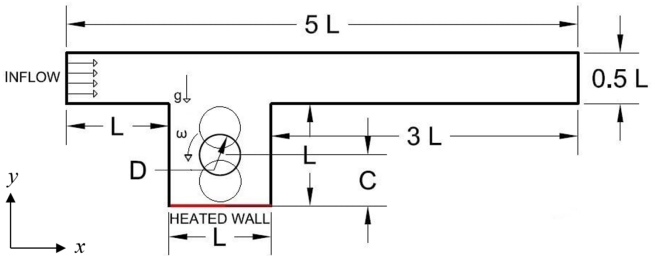

Fig. 1: Sketch of the geometry.

Where L is the length ($L = 0.1$ m). The length of the channel from the inlet opening to the cavity leading edge is L, while $3L$ is the length of the channel behind the cavity trailing edge in the streamwise direction, the height of the channel is $0.5L$, and D is a diameter of the cylinder. The inflow direction is from left to right, with a uniform velocity and a constant temperature T_∞ at $x = 0$. The outflow boundary condition is assumed, located at, $x = 5L$ and the non-slip boundary condition is applied for the rest of the boundaries. The cavity is heated from below at a constant temperature, and the remaining walls of the cavity, cylinder, and channel are adiabatic. The Prandtl number for airflow ($Pr = 0.7$). The Reynolds number is set ($Re = 100$), while the Richardson number range is ($0.1 \leq Ri \leq 10$) and the rotational velocity of the cylinder ($0.5 \leq \omega \leq 4$) rad/sec with the vertical location of the cylinder ($C = 70, 50, 30$) mm. The thermophysical properties of airflow are assumed to be constant, except for

the change in fluid density with temperature, according to the Boussinesq approximation.

2.2. Governing equations

The flow and heat transfer are assumed to be two-dimensional, incompressible, laminar, and steady state. The fluid is air, except for temperature-related changes in fluid density according to the Boussinesq approximation, thermophysical parameters should be constant in this range. The Navier-Stokes equations for mass, momentum, and energy in the Cartesian coordinates are as follows:

Continuity equation:

$$\frac{\partial u}{\partial x}+\frac{\partial v}{\partial y}=0 \tag{1}$$

Momentum equations can be written as:

X-momentum equation:

$$u\frac{\partial u}{\partial x}+v\frac{\partial u}{\partial y}=-\frac{1}{\rho}\frac{\partial p}{\partial x}+\frac{\mu}{\rho}\left(\frac{\partial^2 u}{\partial x^2}+\frac{\partial^2 u}{\partial y^2}\right) \tag{2}$$

Y-momentum equation:

$$u\frac{\partial v}{\partial x}+v\frac{\partial v}{\partial y}=-\frac{1}{\rho}\frac{\partial p}{\partial y}+\frac{\mu}{\rho}\left(\frac{\partial^2 v}{\partial x^2}+\frac{\partial^2 v}{\partial y^2}\right)+\rho\beta\,(T-T_{in}) \tag{3}$$

Energy equation for fluid:

$$u\frac{\partial T}{\partial x}+v\frac{\partial T}{\partial y}=\frac{k}{\rho\ cp}\left(\frac{\partial^2 T}{\partial x^2}+\frac{\partial^2 T}{\partial y^2}\right) \tag{4}$$

Dimensionless parameters:

$$Re=\frac{\rho\ u_{in}\ D_h}{\mu}$$

For non-circular cross-section channels, the hydraulic diameter was described as:

$$D_h=\frac{4A}{p},\quad Ri=\frac{Gr}{Re^2},\quad Gr=\frac{g\beta(T_s-T_{in})L^3}{\vartheta^2},\quad Pr=\frac{\vartheta}{\alpha}$$

Thermal parameters:

The average Nusselt number at the bottom wall is:

$$\overline{Nu}=\frac{1}{L}\int_0^L Nu_L\,dx \tag{5}$$

The local Nusselt number is calculated based on the cavity height *L*.

$$Nu=-\frac{L}{\Delta T}\frac{\partial T}{\partial y}|_{wall} \tag{6}$$

Where,

$$\Delta T=T_{hot}-T_{bulk}$$

Boundary Conditions:

1. $u=u_i,\ v=0,\ T=T_{in}$ at the inlet
2. $\frac{\partial u}{\partial x}=0$ at the exit

   The outflow boundary condition is assumed
3. The cavity is heated from below at a constant temperature, $T_h=constant$
4. The insulated angular velocity (ω) is $(0.5-2-4)$ rad/s with direction counterclockwise. The remaining walls of the cavity and channel are adiabatic $u=0$, $v=0$, $Heat\,flux=0$

3. Numerical method

The results were obtained using ANSYS-FLUENT, an independent approach (2019 R1). Applying local grid refinement close to the walls shows that a grid size of about, 54048 triangular elements is suitable for accuracy and resolution. Additionally, second-order upwind is used for momentum and energy advection. To ensure mass conservation and avoid pressure-velocity decoupling, the Simple Method for Pressure-Linked Equations (Semi Implicit Method for Pressure Linked Equation) was used. To reach the aim of convergence acceleration, all residuals were subjected to the convergence criterion of 10^{-6}. A computational model is validated by comparing the present result of *Nu* with the results presented by Burgos et al. [13].

Table 1: A computational model was validated by comparing the present result of *Nu* and the results provided by Burgos et al. [13].

Parameter	**Present study**	**Burgos et al.**	**Error**
Ri	*Nu*	*Nu*	%
0.01	1.283	1.347	4.9
0.1	1.514	1.507	0.46
1	2.559	2.586	1
10	4.034	4.202	4

4. Results and discussion

For various values of the dimensionless parameter Richardson number, dimensional angular velocity, and location of a circular cylinder, the findings which are displayed as streamlines and isotherms contours together with the Nusselt number, are presented and analyzed in this section. The mixed convection phenomenon in a channel cavity assembly is caused by the combined effect of forced convection caused by airflow inside the channel and rotating cylinder inside the cavity, and natural convection, or buoyancy force, caused by the temperature gradient between the cold airflow and the local heat source embedded at the bottom wall of the cavity.

4.1. Flow field and isotherms

Figure 2 shows the effect of cylinder location on the streamlines at $\omega = 0.5$ rad/sec (CCW), $Re = 100$ and $Ri = 1$. For $C = 70$ mm, a large cell formed on the left side of the lower cavity corner, with the appearance of another one at the upper corner of the same side. For $C = 50$ mm, the streamlines are uniformly distributed in most parts of the cavity, with the formation of vortices on the right and left sides near the cavity opening. For $C = 30$ mm, high-intensity streamlines inside the cavity with the appearance of a vortex at the top of the cylinder. The contour of temperature is shown in Fig. 3. For $C = 70$mm, there are slight curvatures of the thermal dense near the hot surface, while at $C = 50$ mm, an increase in the thermal density curvature towards the right side. For $C = 30$ mm, we observe a slight heat distribution near the hot wall. Figure 4 shows the distribution of streamlines when $\omega = 2$ rad/sec (CCW), $Re = 100$, and $Ri = 0.1$. It can be seen that for $C = 70$ mm, a large cell forms at the bottom of the cylinder area, in addition to forming a small cell in the top left part of the cavity due to the effect in pressure values and the intensity of the streamlines in space near the cylinder surface increases. For $C = 50$ mm (the cylinder is at the center of the cavity) as can be seen vortices are formed, the first at the top and the second at the bottom on the left side of the cavity, with an increase in the density of the streamlines when approaching the cylinder surface, due to the effect of cylinder rotation. For $C = 30$ mm, we notice the formation of a large cell at the top of the cylinder near the opening of the cavity, because of the secondary flow, the fluid mixes and forms a circulating cell. As for the isotherm profiles of Fig. 5, when $C = 70$ mm, we note that the thermal density is evenly distributed along the hot surface. This is due to that when the cylinder becomes closer to the top of the open cavity, the temperature gradient reduces near the hot surface, while at $C = 50$ mm, thermal density at the right of the hot surface and a noticeable thermal distribution within the cavity towards the exit region, as a result of increasing the effect of rotation of the cylinder at this location. For $C = 30$ mm, the isotherm zone appears at the right part of the cavity. Figure 6, shows the effect of cylinder location on the streamlines at $Re = 100$, $Ri = 1$, and $\omega = 2$ rad/sec (CCW). It can be seen that for $C = 70$ mm, a large cell forms at the bottom of the cylinder area, in addition to forming a small cell in the top left part of the cavity due to the effect in pressure values and the intensity of the streamlines in space near the cylinder surface increases. For $C = 50$ mm (the cylinder is at the center of the cavity) as can be seen vortices are formed, the first at the top and the second at the bottom on the left side of the cavity, with an increase in the density of the streamlines when approaching the cylinder surface, due to the effect of cylinder rotation. For $C = 30$ mm, we notice the formation of a large cell at the top of the cylinder near the opening of the cavity, because of the secondary flow, the fluid mixes and forms a circulating cell. As for the isotherm profiles of Fig. 7, when $C = 70$ mm, note that the thermal density is evenly distributed along the hot surface. This is due to that when the cylinder becomes closer to the top of the open cavity, the temperature gradient reduces near the hot surface, while at $C = 50$ mm, thermal density at the right of the hot surface and a noticeable thermal distribution within the cavity towards the exit region, as a result of increasing the effect of rotation of the cylinder at this location. Figure 8, represents the streamlines contour for $Re = 100$, $Ri = 10$, $\omega = 2$ rad/s (CCW). For $C = 70$ mm, the intensity of streamlines increases at the bottom of the cylinder towards the walls of the cavity, with a vortex in the lower half of the cavity below the cylinder, due to the effect of pressure gradient in this area. For $C = 50$ mm, a vortex is formed below the right cavity angle with an increase in the intensity of the lines of flow at the walls of the cavity towards the cylinder wall. For $C = 30$ mm, it is clear to show the formation of a fairly large vortex at the upper half of the cavity above the cylinder, with a small vortex below the left of the cavity. Through temperature profile Fig. 9, the inner rotating circular cylinder locations have a small effect on the isotherms when the circular cylinder moves upward $C = 70$ mm, we note the curvature of the heat distribution from the plane of the heated surface towards the left of the cavity, due to the effect of buoyancy force. For $C = 50$ mm, notice a decrease in the thermal density along the hot surface, in this case, the location of the cylinder has the effect of improving the temperature gradient inside the cavity. For $C = 30$ mm, the heat distribution occurs near the hot surface compared to the first and second positions of the cylinder when $C = 70,\ 50$ mm. In this case, the buoyancy forces effect becomes greater than the effects of the rotating circular cylinder and force flow at different locations of the circular cylinder, so the natural convection is dominant. For $C = 30$ mm, the isotherm zone appears at the right part of the cavity. For $Re = 100$, $Ri = 1$, and $\omega = 4$ rad/s (CCW), is illustrated in Fig. 10. For the streamlines, when $C = 70$ mm, it can be seen from this figure the intensity of the streamlines is increased gradually from the rotation cylinder towards the vertical walls of the cavity, also a large cell is occurred at the bottom space of the rotation cylinder, due to the effect of pressure gradient in this region. For $C = 50$ mm, it can be noted a small vortex on the left side at the corner of the cavity is formed with an increase in the intensity of the streamlines around the surface of the cylinder. For $C = 30$ mm, the intensity of the streamlines is higher than that of other locations, with the appearance of a small cell formed at the space near the top of the rotation cylinder. Through the contour of the temperature shown in Fig. 11. It can be seen from this figure the thickness of the thermal boundary layer is increased when the cylinder is located near the hot surface and decreases when the cylinder is at the center of the cavity.

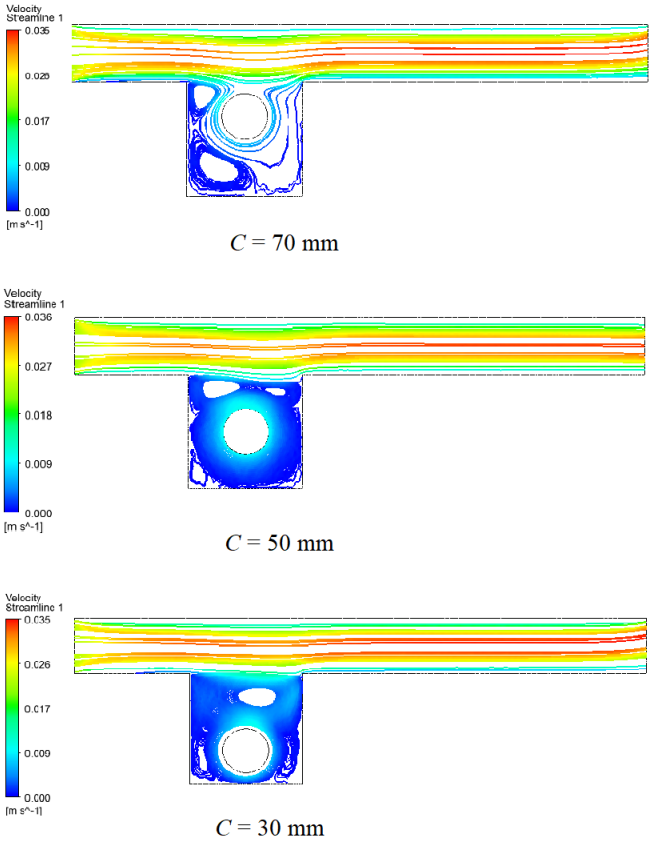

Fig. 2: Streamlines contours at $Ri = 1$, $\omega = 0.5$ rad/s

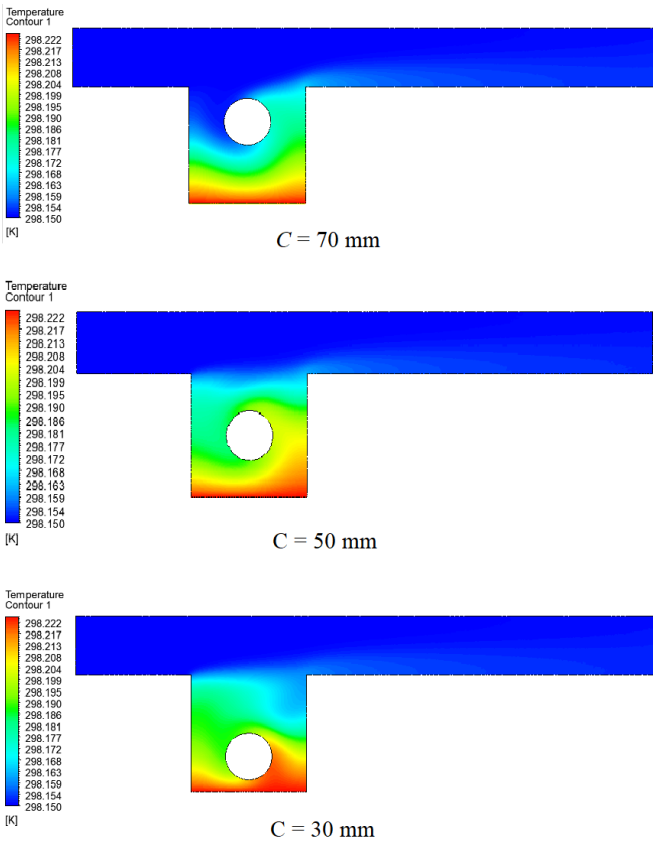

Fig. 3: Isotherms contours at $Ri = 1$, $\omega = 0.5$ rad/s

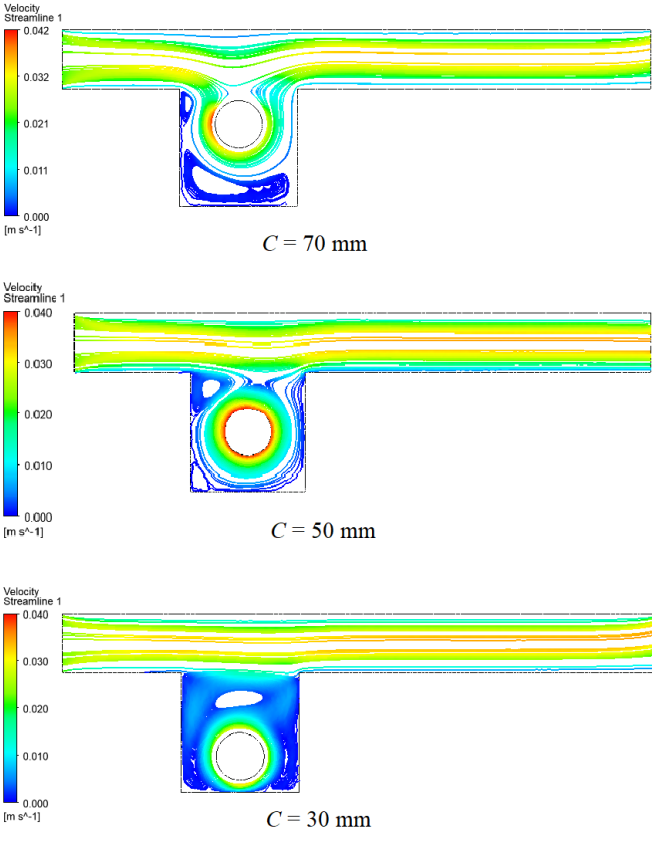

Fig. 4: Streamlines contours at $Ri = 0.1$, $\omega = 2$ rad/s

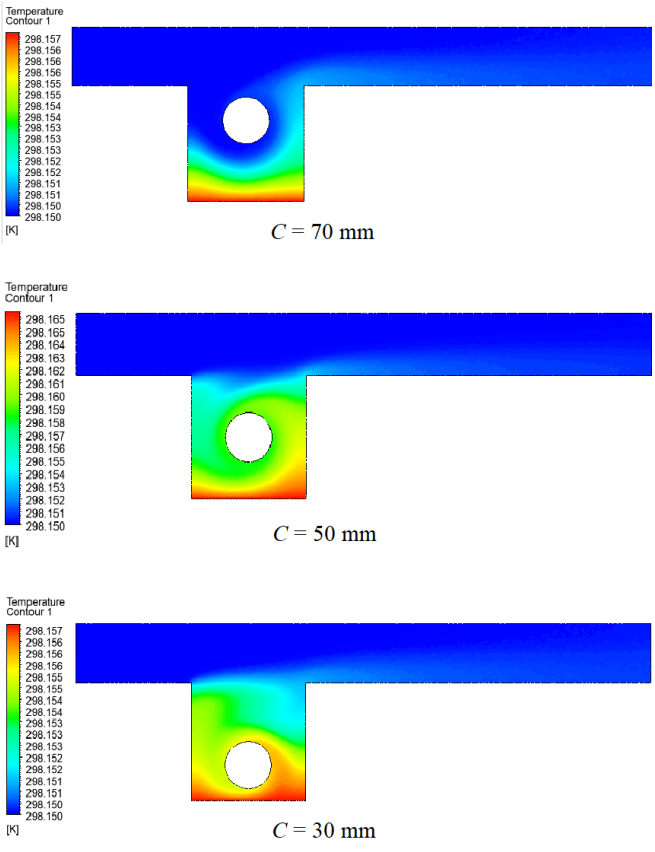

Fig. 5: Isotherms contours at $Ri = 0.1$, $\omega = 2$ rad/s

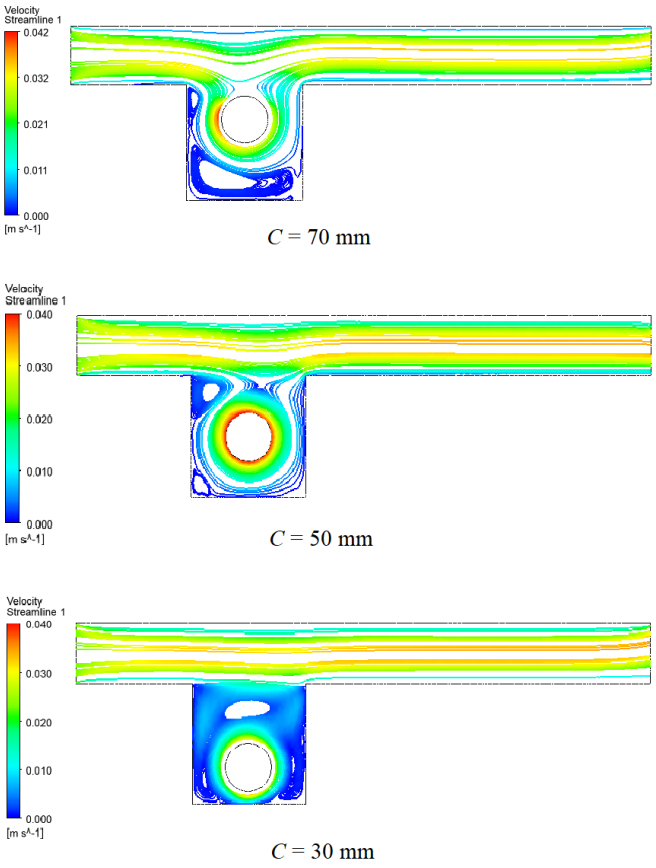

Fig. 6: Streamlines contours at $Ri = 1$, $\omega = 2$ rad/s

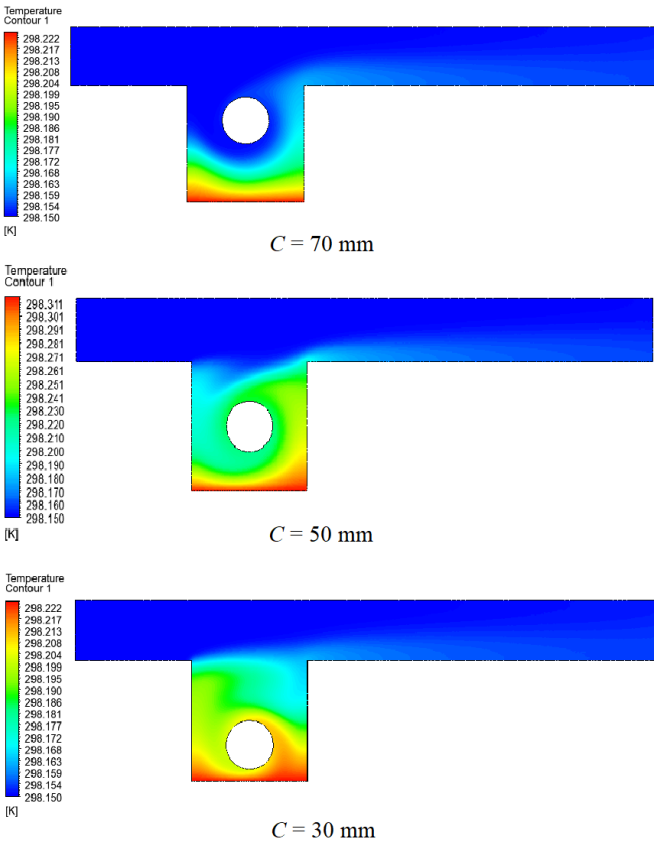

Fig. 7: Isotherms contours at $Ri = 1$, $\omega = 2$ rad/s

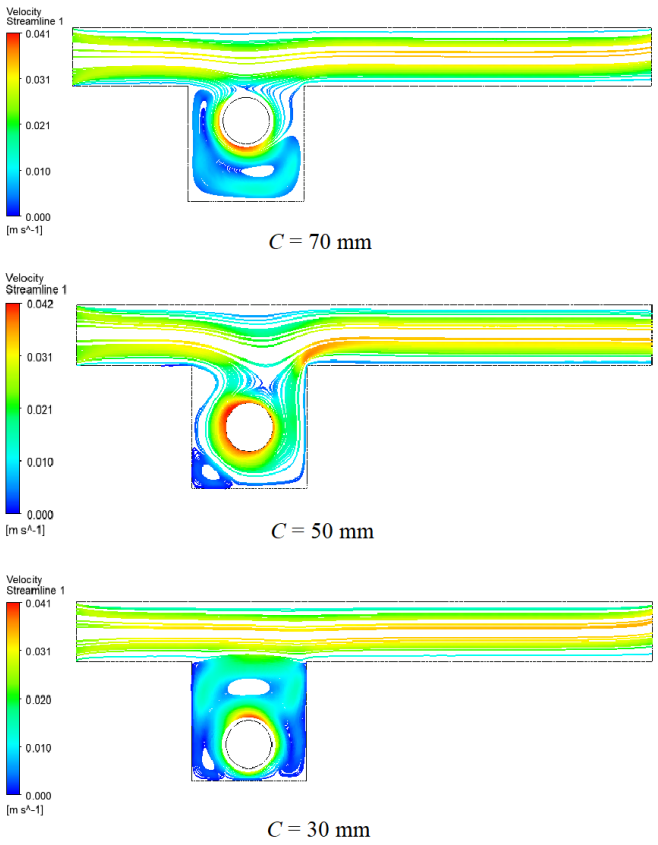

Fig. 8: Streamlines contours at $Ri = 10$, $\omega = 2$ rad/s

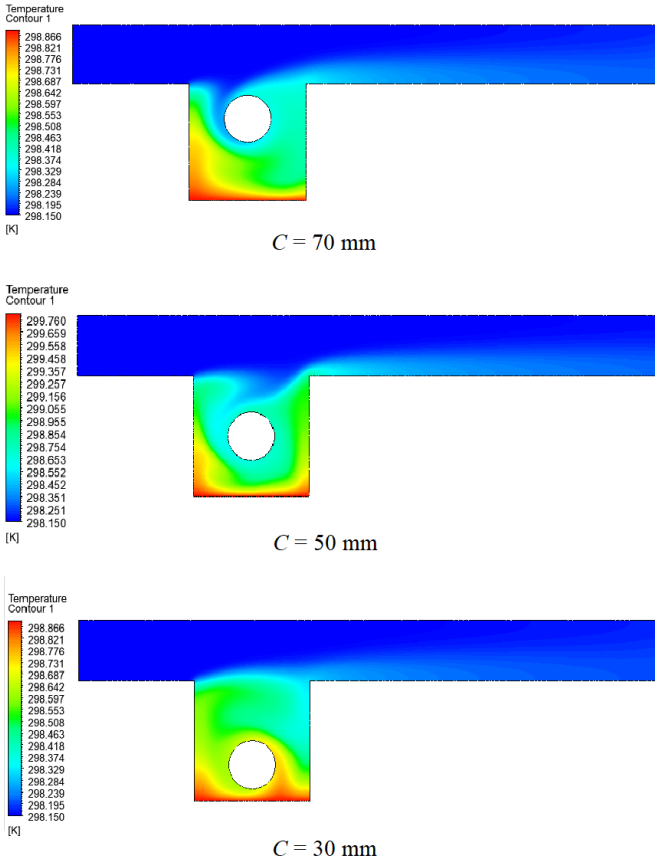

Fig. 9: Isotherms contours at $Ri = 10$, $\omega = 2$ rad/s

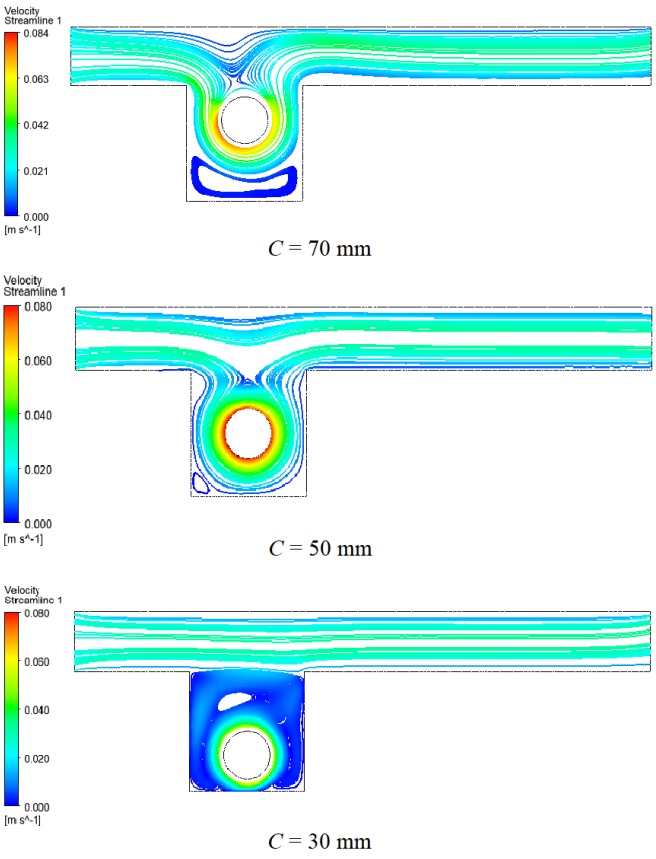

Fig. 10: Streamlines contours at $Ri = 1$, $\omega = 4$ rad/s

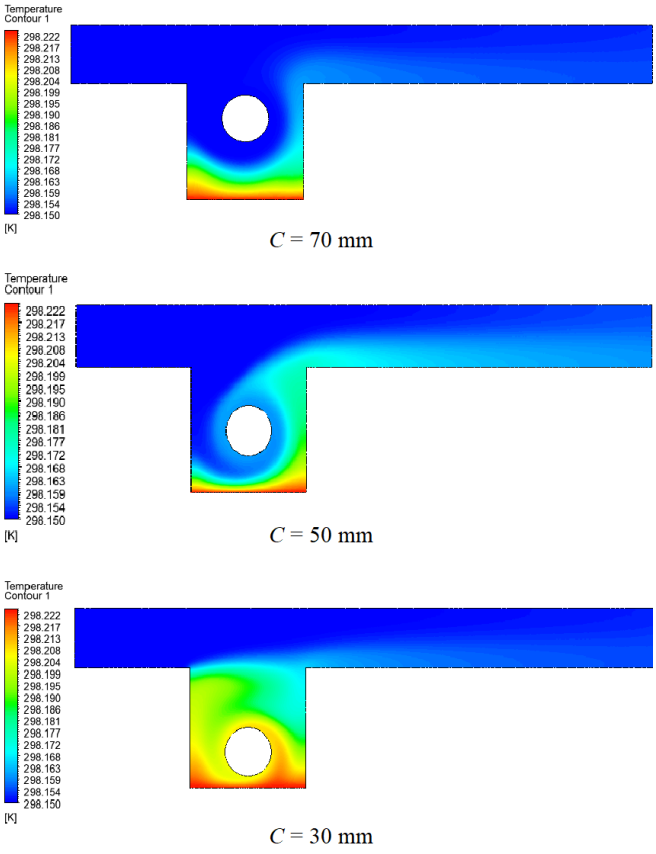

Fig. 11: Isotherms contours at $Ri = 1$, $\omega = 4$ rad/s

4.2. Nusselt number

Figure 12 shows the effect of increasing the rotational speed of the cylinder on the local Nusselt values according to the position of the cylinder inside the cavity at $Ri = 1$, $Re = 100$. For $\omega = 0.5$ rad/sec at this angular velocity for $C = 70$ mm, a gradual rise of the Nusselt curve until it reaches its highest value on the left of the hot surface, followed by a gradual decrease of the curve on the right side of the hot surface. As for the Nusselt values curve when the cylinder position is at 50 and 70 mm, a gradual rise on the left side is followed by a gradual decrease on the right of the hot surface. For $\omega = 2$ rad/sec, also it can be seen from this figure, that the effect of angular velocity behaves the same as that in the case of $\omega = 0.5$ rad/sec, but for $C = 50$ mm, a significant increase of the Nusselt values curve on the left side of the hot surface compared to the previous case. For $\omega = 4$ rad/sec, it is clear from this figure that we have a similar trend as that in the case of $\omega = 2$ rad/sec, but the value of the local Nusselt number is higher because of the effect of increase angular velocity of the cylinder inside the cavity. The inner rotating circular cylinder locations have a small effect when the rotating circular cylinder moves upward until $C = 70$ mm, or when it moves downward until $C = 30$ mm, and the effect of forced convection dominates. Figure 13 predicts the variation of local Nusselt values (along the hot surface) with the location of the cylinder within the cavity at the angular velocity $\omega = 2$ rad/sec, $Re = 100$. When $Ri = 0.1$, For $C = 30$ mm, notice a gradual increase on the left side of the hot surface until it reaches its highest value near the surface on the left side of the cylinder after that, a gradual decrease of the Nusselt values curve occurs on the right side of the hot surface. For $C = 50$ mm, it can be seen a gradual increase of the Nusselt curve on the left side due to the high-temperature gradient at this region with a gradual decrease of the curve on the right side of the hot surface, due to increasing the resistance to fluid flow in this area. For $C = 70$ mm, we observe a (approximately) symmetrical Nesselt values curve on the left and right sides of the hot surface. $Ri = 10$, shows a similar trend as that in the case of $Ri = 0.1$ with the values of local Nusselt number being higher with selected upward, center, and downward rotating circular cylinder locations, due to the great influence of thermal convection heat transfer and the effect of buoyancy force with increase Ri.

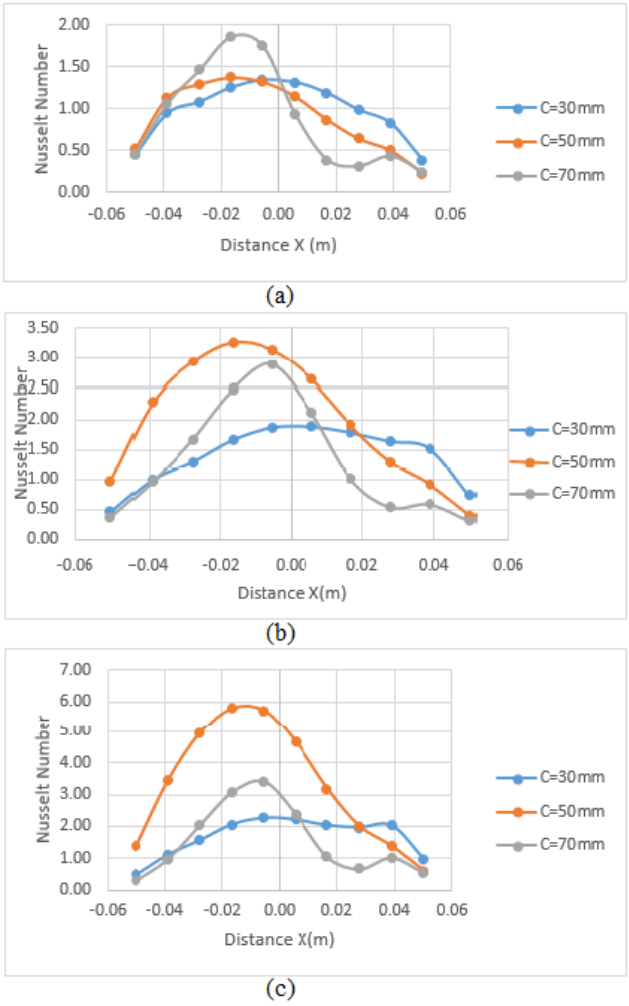

Fig. 12: Variation of Nusselt number along the heated surface at $Ri = 1$, (a) $\omega = 0.5$ rad/sec, (b) $\omega = 2$ rad/sec, (c) $\omega = 4$ rad/sec

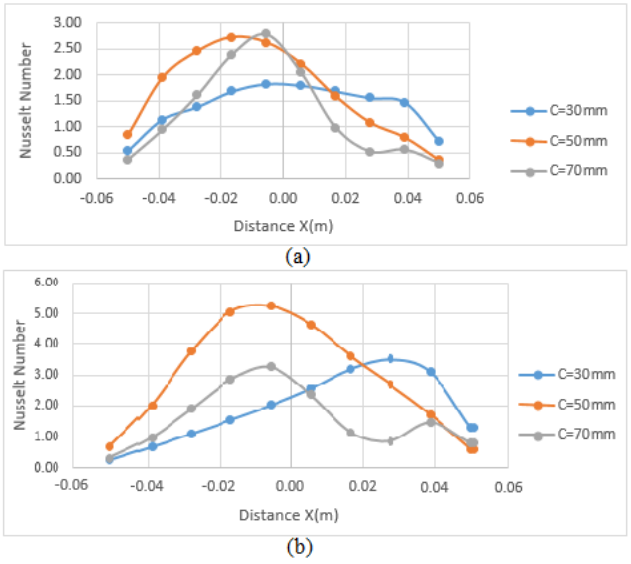

Fig. 13: Variation of Nusselt number along the heated surface at $\omega = 2$ rad/sec, (a) $Ri = 0.1$, (b) $Ri = 10$

5. Conclusions

For the mixed convective flow over a 2D square open cavity heated from below and containing a rotating cylinder, numerical simulation has been performed. The effects of Reynolds number ($Re = 100$), Richardson number ($Ri = 0.1, 1, 10$), and investigated the effect of the locations ($C = 70, 50, 30$) mm of the cylinder on the fluid flow and heat transfer in the square cavity for different cylinder rotation ($\omega = 0.5, 2, 4$) rad/s.

1. Increasing the average Nusselt values with increasing the angular velocity of the cylinder inside the cavity.
2. It was found that the thickness of the thermal boundary layer decreases with the increase in the rotational speed of the cylinder and thus improves the heat transfer process.
3. The best results obtained with the values of average Nusselt are when the position of the cylinder is in the center of the cavity to give the best heat transfer process.
4. The development of the temperature distribution inside the cavity towards the exit region increases with the increase in the angular velocity of the cylinder.
5. For all cylinder locations, the average Nusselt number increases as Ri increases.

Nomenclature		
Symbol	Description	SI Units
C	Location of circular cylinder	mm
Cp	Specific heat of air at constant pressure	J/kg.K
D	Dimensional cylinder length	mm
Dh	Hydraulic diameter	mm
Gr	Grashof number	-
g	Gravitational acceleration	m/s^2
k	Thermal conductivity of fluid	W/m.K
L	Length of the enclosure	mm
Nu	Nusselt number	-
$\overline{Nu}$	Average Nusselt number	-
p	Pressure	N/m^2
Pr	Prandtl number	-
Re	Reynolds number	-
Ri	Richardson number	-
T	Temperature	K
Th	Hot temperature	K
T_{in}	Inlet temperature	K
T_∞	Temperature of free stream	K
u, v	Cartesian velocity components	m/s
X, Y	Cartesian coordinates	-
Greek Symbols		
Symbol	Description	SI Units
ω	Angular velocity	rad/sec
ρ	Density of the fluid	kg/m^3
μ	Dynamic viscosity	kg/m.s
β	Thermal expansion coefficient	1/K
ν	Kinematic viscosity	m^2/s
α	Thermal diffusivity	m^2/s

References

[1] G. Smaisim, O. Fatla, A. Valera Medina, A. Rageb, and N. Syred, "Experimental and theoretical investigation of the effect of rotating circular cylinder speed on the lift and drag forces," *International Journal of Energy and Environment*, vol. 7, no. 1, pp. 23–36, 2016.

[2] S. M. Shrama, "Numerical analysis of mixed convection heat transfer for laminar flow in a channel with an open cavity," *Al-Qadisiyah Journal for Engineering Sciences*, vol. 4, no. 4, pp. 419–438, 2011.

[3] Y.-C. Shih, J. Khodadadi, K.-H. Weng, and H. Oztop, "Transient leading to periodic fluid flow and heat transfer in a differentially-heated cavity due to an insulated rotating object," in *Heat Transfer Summer Conference*, vol. 42746, 2007, pp. 333–342.

[4] S. M. Shrama, F. A. Abood, and Z. K. Radhi, "Study of mixed convection heat transfer inside a vented square cavity with inner heated cylinder," *University of Thi-Qar Journal for Engineering Sciences*, vol. 2, no. 3, pp. 113–130, 2011.

[5] A. K. Alshara, "Effect of single or multi rotating horizontal cylinders on the mixed convection heat transfer inside a triangular enclosure," *Al-Qadisiyah Journal for Engineering Sciences*, vol. 5, no. 1, 2012.

[6] K. Khanafer and S. Aithal, "Laminar mixed convection flow and heat transfer characteristics in a lid driven cavity with a circular cylinder," *International Journal of Heat and Mass Transfer*, vol. 66, pp. 200–209, 2013.

[7] F. A. Abood, A. K. Alshara, and H. A. Al-mayahi, "Mixed convection heat transfer inside a vented square enclosure with concentric rotation inner cylinder," *University of Thi-Qar Journal for Engineering Sciences*, vol. 4, no. 3, pp. 60–76, 2013.

[8] F. Selimefendigil and H. F. Öztop, "Effect of a rotating cylinder in forced convection of ferrofluid over a backward facing step," *International Journal of Heat and Mass Transfer*, vol. 71, pp. 142–148, 2014.

[9] K. Khanafer, S. Aithal, and K. Vafai, "Mixed convection heat transfer in a differentially heated cavity with two rotating cylinders," *International Journal of Thermal Sciences*, vol. 135, pp. 117–132, 2019.

[10] S. Mehryan, E. Izadpanahi, M. Ghalambaz, and A. Chamkha, "Mixed convection flow caused by an oscillating cylinder in a square cavity filled with cu–al2o3/water hybrid nanofluid," *Journal of Thermal Analysis and Calorimetry*, vol. 137, no. 3, pp. 965–982, 2019.

[11] Z. Salman, F. Aiss, and M. Almudhaffar, "Experimental study of mixed convection in a cavity with a rotating cylinder," *Journal of Advanced Research in Fluid Mechanics and Thermal Sciences*, vol. 74, no. 2, pp. 16–26, 2020.

[12] F. Selimefendigil and H. F. Öztop, "Mixed convection in a pcm filled cavity under the influence of a rotating cylinder," *Solar Energy*, vol. 200, pp. 61–75, 2020.

[13] J. Burgos, I. Cuesta, and C. Salueña, "Numerical study of laminar mixed convection in a square open cavity," *International Journal of Heat and Mass Transfer*, vol. 99, pp. 599–612, 2016.